

Computer simulation and software engineering in optical analysis of phosphor-converted white light-emitting diodes utilizing barium sulfate

Le Thi Trang¹, Nguyen Thi Phuong Loan², Pham Hong Cong³, Nguyen Doan Quoc Anh⁴, Hsiao-Yi Lee⁵

¹Faculty of Information Technology, Dong Nai Technology University, Dong Nai, Vietnam

²Faculty of Fundamental 2, Posts and Telecommunications Institute of Technology, Ho Chi Minh City, Vietnam

³Faculty of Electrical Engineering Technology, Industrial University of Ho Chi Minh City, Ho Chi Minh City, Vietnam

⁴Faculty of Electrical and Electronics Engineering, Ton Duc Thang University, Ho Chi Minh City, Vietnam

⁵Department of Electrical Engineering, National Kaohsiung University of Science and Technology, Kaohsiung City, Taiwan

Article Info

Article history:

Received Apr 22, 2025

Revised Sep 30, 2025

Accepted Nov 7, 2025

Keywords:

Barium sulfate

Color rendering index

Computer simulation

Luminous efficacy

Software engineering

White LED

ABSTRACT

Achieving uniform nanoparticle dispersion in electrospun polymer nanofibers remains a critical challenge, as conventional electrospinning often leads to particle agglomeration and nozzle clogging, reducing fiber uniformity and functional efficiency. This study explicitly addresses this problem by developing poly (vinyl alcohol) (PVA)/BaSO₄ composite nanofibers through both conventional and ultrasonic-assisted electrospinning. Scanning electron microscopy (SEM) revealed that ultrasonication effectively disrupted nanoparticle agglomerates, yielding smoother and more uniform fiber morphologies. X-ray diffraction (XRD) analysis further confirmed that ultrasonic processing reduced the crystalline intensity of PVA and BaSO₄, indicating enhanced polymer–filler interaction and finer BaSO₄ distribution. Quantitatively, the agglomeration slope decreased from 0.039 (conventional) to 0.006, and the mean crystallite size was reduced from approximately 470 to 300 nm. These results are consistent with recent advances showing that ultrasonic electrospinning improves nanoparticle dispersion and stability in polymer matrices, thereby enhancing optical and mechanical properties. Ultimately, this work demonstrates that ultrasonic-assisted electrospinning provides a robust and scalable strategy to fabricate lightweight, flexible, and multifunctional PVA-based radiation-shielding materials with superior nanoparticle dispersion and structural homogeneity.

This is an open access article under the [CC BY-SA](#) license.



Corresponding Author:

Nguyen Thi Phuong Loan

Faculty of Fundamental 2, Posts and Telecommunications Institute of Technology

Ho Chi Minh City, Vietnam

Email: ntploan@ptithcm.edu.vn

1. INTRODUCTION

Electrospinning has garnered considerable interest owing to its capacity to produce polymer fibers with diameters spanning from nanometers to several micrometers, utilizing either polymer liquids or solutions. It provides a comparatively straightforward and economical method in contrast to traditional fiber-processing techniques, while enabling the production of porous structures advantageous for filtration, sensing, biomedical scaffolds, and optoelectronic applications [1]–[4]. In particular, research on composite nanofibers integrating functional nanomaterials such as metal nanoparticles, clays, carbon nanotubes, and

ceramics has swiftly advanced, owing to their distinctive physicochemical properties [5]–[8]. Nevertheless, nanoparticle agglomeration continues to pose a significant challenge, potentially diminishing the performance of these hybrid fibers by impairing their mechanical, thermal, and optical properties [9], [10].

Conventional electrospinning relies on an applied high voltage to stretch a polymer jet from the syringe tip toward a collector. While effective, this method often suffers from poor nanoparticle dispersion and nozzle clogging when processing viscous or nanoparticle-rich solutions [11]. Earlier mixed-polymer nanofiber studies frequently reported severe clustering of inorganic fillers and unstable jet flow, which resulted in irregular fiber morphologies, large surface defects, and reduced reproducibility. These persistent issues limited the ability to scale up electrospinning for functional nanocomposites, especially when high filler concentrations were required. Ultrasonic electrospinning has recently emerged as a powerful modification to address these drawbacks. By introducing ultrasonic vibrations, this method continuously agitates the polymer solution, reduces surface tension at the nozzle tip, and suppresses agglomeration of nanoparticles, thereby enabling the production of uniform fibers from highly loaded or viscous solutions [12]. In particular, ultrasonication helps to overcome syringe tip clogging by keeping suspended nanoparticles dispersed during jet formation, while simultaneously breaking apart nanoparticle clusters that would otherwise compromise fiber integrity. Recent studies have shown that ultrasonic-assisted electrospinning enables excellent dispersion of hybrid nanoparticles, such as silver and metal oxides, within polymer matrices [13], paving the way for more reliable functional nanofibers.

Parallel to this development, poly (vinyl alcohol) (PVA)-based composite nanofibers have been extensively explored between 2020 and 2025 for applications in environmental, biomedical, and radiation protection technologies due to their processability, biocompatibility, and functional versatility [14]. For instance, PVA/CeO₂ nanofibers have demonstrated improved stability and radiation shielding performance [15], while PVA/magnetite nanofibers have shown effective attenuation of gamma radiation [16]. Similarly, PVA-ZnO-CuO hybrid fibers were recently reported to exhibit both enhanced mechanical properties and radiation shielding capability [17]. These advances also emphasize that effective nanoparticle dispersion remains the bottleneck in maximizing fiber performance, reinforcing the need for methods like ultrasonication that directly target agglomeration and clogging challenges.

In this work, we focus on fabricating PVA/BaSO₄ composite nanofibers using ultrasonic electrospinning. BaSO₄ is a well-known X-ray contrast and radiation-shielding material, yet its uniform incorporation into polymer fibers has been hindered by nanoparticle agglomeration. Here, we explicitly demonstrate that ultrasonication facilitates effective BaSO₄ dispersion, resulting in reduced crystallite size and controlled cluster morphology, as verified through analyses conducted using scanning electron microscopy (SEM) and x-ray diffraction (XRD). The novelty of this study lies in coupling ultrasonic electrospinning with BaSO₄-loaded PVA fibers to achieve uniform particle distribution and tunable structural features, offering new opportunities for high-performance radiation shielding nanofibers [18].

2. METHOD

Barium sulfate (BaSO₄, average particle size approximately 0.43 μm) was sourced from Kanto Chemical Corporation in Japan. PVA with a polymerization degree of 1,700 and 88% hydrolysis was supplied by Kuraray Corporation Ltd in Japan. Distilled water was utilized as the solvent in all preparations of polymer solutions. The PVA concentration was consistently maintained at 12 wt% across all formulations, while the BaSO₄ loading was systematically altered from 2.5 to 60 wt% in relation to PVA to examine the influence of filler content on fiber morphology and particle dispersion. The PVA solution was formulated by dissolving PVA granules in distilled water with continuous agitation at 80 °C until fully dissolved. After cooling to ambient temperature, specified quantities of BaSO₄ particles were incorporated into the 12 wt% PVA solution and thoroughly mixed through vigorous agitation, producing stable suspensions of PVA/BaSO₄ mixtures. These suspensions were employed directly in the electrospinning process [19].

Electrospinning was performed using a custom setup consisting of a micro-syringe pump connected to a 30 mL glass syringe, a high-voltage power supply, and an ultrasonic vibrating device integrated into the nozzle. The electrospinning nozzle consisted of a metallic capillary tip with an internal diameter of 0.9 mm. The following electrospinning parameters were applied:

- Applied voltage: 10 kv.
- Tip-to-collector distance (TCD): 10 cm.
- Solution flow rate: 0.1 ml/hr.
- Ultrasonic frequency: 17.5-20.5 kHz.

The incorporation of ultrasonic vibration at the nozzle continuously agitated the solution, thereby improving BaSO₄ dispersion and minimizing particle agglomeration during fiber formation [20]. The morphology of the fibers was examined via SEM, while energy-dispersive x-ray spectroscopy (EDX) attached to the SEM was used for elemental mapping to confirm the distribution of Ba and S elements within

the fibers. The chemical structure and polymer-filler interactions were analyzed through Fourier-transform infrared spectroscopy (FTIR) and XRD analyses. The spatial distribution of BaSO₄ particles inside the fibers was quantified through SEM image analysis (minimum 50 measurements, assuming spherical aggregates), complemented by EDX mapping to visualize homogeneity.

3. RESULTS AND DISCUSSION

The morphology of PVA/BaSO₄ composite nanofibers fabricated by conventional and ultrasonic electrospinning was analyzed by SEM and transmission electron microscopy (TEM). TEM images revealed that most BaSO₄ particles were positioned on the outer surfaces of the nanofibers rather than being fully embedded within, which can be attributed to the relatively large BaSO₄ particle size compared with the fiber thickness. Notably, fibers produced via ultrasonic electrospinning exhibited better particle separation and significantly fewer agglomerates than those prepared by conventional electrospinning. This demonstrates that ultrasonication effectively disrupted and redistributed highly accumulated BaSO₄ particles during fiber formation [21]. The dispersion of BaSO₄ within the PVA matrix was quantitatively evaluated using the particle agglomeration index. SEM results showed that the slope of cluster size growth was ~0.039 for conventional electrospinning but decreased sharply to only 0.006 for ultrasonic electrospinning. This substantial reduction highlights the efficiency of ultrasonic treatment in suppressing agglomeration and promoting uniform nanoparticle dispersion. Although cluster dimensions varied slightly with filler content, the overall trend confirmed that ultrasonication consistently improved filler distribution without introducing unwanted artifacts.

The influence of BaSO₄ addition on fiber morphology was further investigated. Both conventional and ultrasonic electrospinning produced fibers with comparable average diameters, indicating that fiber size was not directly affected by ultrasonic treatment. Instead, the primary factor was the increasing BaSO₄ content, which reduced the effective fraction of PVA, thereby decreasing the average fiber diameter. These results confirm that ultrasonic electrospinning enhances nanoparticle dispersion without altering the fundamental fiber formation mechanisms. XRD was employed to assess the crystallinity of the composites. Strong PVA diffraction peaks at 19.5° and 24.5° (corresponding to the (101) and (200) planes) were observed, along with distinct BaSO₄ maxima. In samples produced via ultrasonic electrospinning, the relative intensity of BaSO₄ diffraction peaks decreased notably at filler contents ≤15 wt%, suggesting disruption of crystallite ordering and improved dispersion. The mean BaSO₄ crystallite size was ~470 nm for conventional samples but reduced to ~300 nm for ultrasonic electrospun samples, confirming crystallite size refinement induced by ultrasonic energy. At higher loadings (>20 wt%), BaSO₄ particles tended to collide and form secondary agglomerates via van der Waals forces, increasing diffraction intensity and partially restoring crystallinity. Concurrently, attenuation of the PVA crystal peaks was observed, likely due to disruption of polymer chain ordering caused by continuous ultrasonic vibrations acting on intermolecular linkages. Similar effects on BaSO₄ diffraction maxima in the monoclinic phase were reported in prior studies. Overall, these findings demonstrate that ultrasonic electrospinning is an efficient approach to disturb crystalline micro-forms, reduce BaSO₄ crystallite size, and achieve more homogeneous distribution compared with conventional methods. From a functional standpoint, BaSO₄ incorporation provided dual advantages. First, its high atomic number and density enhanced X-ray attenuation, highlighting its potential as a radiation-shielding filler or X-ray contrast agent in biomedical applications. Second, BaSO₄ significantly improved optical performance. Luminous flux measurements showed that PVA/BaSO₄ nanofiber composites reached a maximum luminous flux of 174.8 lm at 50 wt% BaSO₄ loading, making them particularly suitable for high-brightness white light-emitting diode (WLED) applications [22], [23].

Finally, a comparison with other commonly used additives such as ZnO and TiO₂ demonstrated that BaSO₄ exhibited superior luminous flux performance under comparable conditions. Although ZnO and TiO₂ are extensively researched for their roles in light scattering and luminosity improvement, their contributions are comparatively lower than those of BaSO₄ within similar polymer systems. This performance advantage, combined with biocompatibility and radiation shielding properties, positions BaSO₄ as a highly effective multifunctional additive for next-generation nanofiber-based optical, biomedical, and radiation-protection applications. For example, the Debye-Scherrer method in (1) was employed to analyze the full width at half-maximum (FWHM) of the most prominent and characteristic peak (140) in order to estimate the mean crystallite size. Here, λ denotes the X-ray wavelength (1.5402 Å), and β is the shape factor, typically assigned a value of 0.89. D represents the average crystallite dimension in angstroms, θ is the Bragg angle measured in degrees, and β indicates the entire FWHM of the most significant peak in radians when the shape factor is uncertain. The average BaSO₄ crystal dimension (~15 wt%) of the synthesized PVA/BaSO₄ composite nanofibers was determined to be approximately 300 nm, which is smaller than the approximately 470 nm observed in conventional electrospun PVA/BaSO₄ composite nanofibers.

$$D = K\lambda/\beta \cos \theta \quad (1)$$

Figure 1 depicts the correlation between BaSO₄ dosage and light distribution. Elevating BaSO₄ content improves wavelength conversion efficiency and light transmission by facilitating forward scattering and minimizing reabsorption losses, resulting in increased blue-light luminosity in forward emission. As the BaSO₄ content increases, the quantity of yellow phosphor is correspondingly adjusted to preserve color equilibrium. Figure 2 demonstrates that the YGA:Ce yellow phosphor dosage rises with increasing BaSO₄ dosage, whereas the phosphor ratio decreases from approximately 5% to nearly 1% as the BaSO₄ content increases from 10 to 50 wt%. Figure 3 illustrates that the correlated color temperature (CCT) exhibits minimal dependence on BaSO₄ concentration; however, a maximum CCT of approximately 6,300 K is observed at 10 wt% BaSO₄, indicating a stable chromaticity condition at moderate doping levels. Finally, Figure 4 demonstrates that the D-CCT value diminishes progressively with increasing BaSO₄ content, attaining its minimum at 50 wt% BaSO₄, approximately 400 K lower than the value observed at 10 wt%, thereby indicating improved angular color uniformity. Overall, increased BaSO₄ concentrations enhance light scattering and spectral uniformity while preserving a consistent CCT. However, excessive loading can lead to backscattering losses and diminished luminous efficacy, suggesting that an optimal BaSO₄ concentration is essential to achieve balanced optical performance.

Figure 5 illustrates that the brightness of white light emission was not always increased by BaSO₄. 50 wt% of BaSO₄ produced the highest yields, whereas 10 wt% produced the lowest. Enhanced backscattering together with repeated reabsorption reduces the amount of blue light emitted and leads to a non-uniform chromatic distribution. Under stronger blue-light backscattering, the phosphor's emission can shift from orange-red toward blue-yellow as the BaSO₄ content increases. Phosphor coating cannot begin to expand until the BaSO₄ concentration is reached. The emission spectrum becomes narrowed because the altered light path undergoes repeated reflections from surrounding surfaces. Stated differently, an increased proportion of back-reflected converted light could result from a high phosphorus dose, increasing CCT at the expense of decreased luminous intensity. It was found that 50 wt% of BaSO₄ was sufficient to improve color consistency and brightness in a simulated WLED that had an approximate lumen output power of 175 lm, as shown in Figure 5.

As depicted in Figures 6 and 7, the BaSO₄ content significantly influences both the luminance and the color-rendering capabilities of WLED systems. Hue rendition was consistently diminished as the BaSO₄ concentration increased to 50 wt%, based on experiments employing the hue rendering index (CRI) and hue quality scale (CQS). The reductions in CRI and CQS may be attributable to the inherently variable characteristics of blue, green, and yellow-orange structures. Greater dispersion and unpredictably elevated BaSO₄ concentrations produce light that progressively transitions toward the yellow-orange region of the spectrum. As we assess the data and account for additional parameters such as particle size, further refinement of the phosphor's CRI and CQS will be undertaken [24], [25]. Figure 8 illustrates the emission bands of BaSO₄. It has been demonstrated that BaSO₄ enhances the orange-red and blue regions of the white light spectrum. To enhance illumination efficiency, the light scattering and absorption characteristics of BaSO₄ can be modified. The wavelength ranges exhibiting the highest peaks are yellow-orange (approximately 550 nm) and blue (approximately 450 nm).

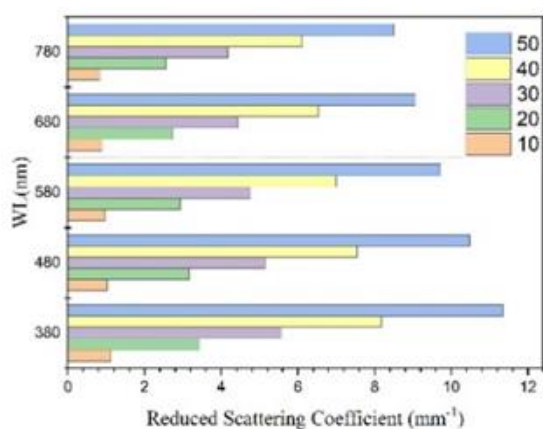


Figure 1. Scattering coefficients with various BaSO₄ proportions

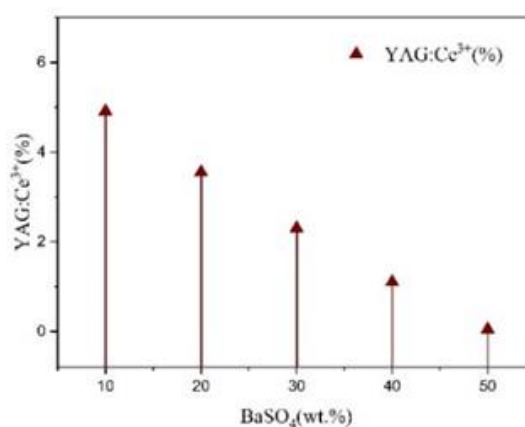


Figure 2. Changes in the YAG:Ce phosphor ratio as the BaSO₄ fraction varies

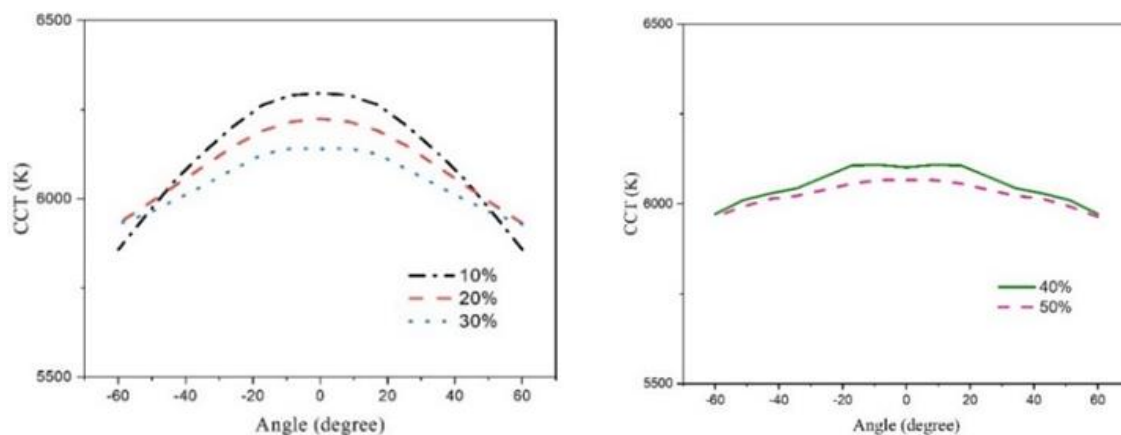
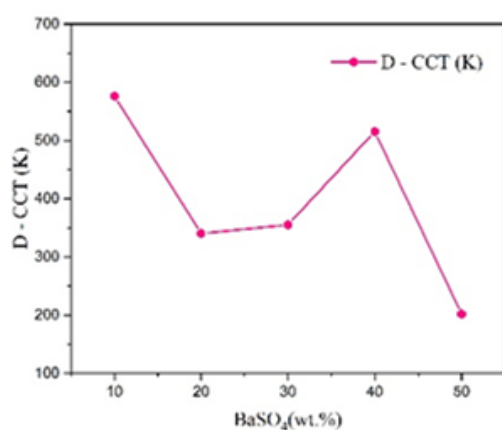
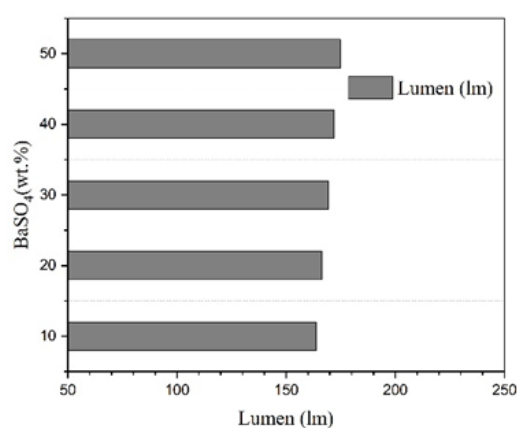
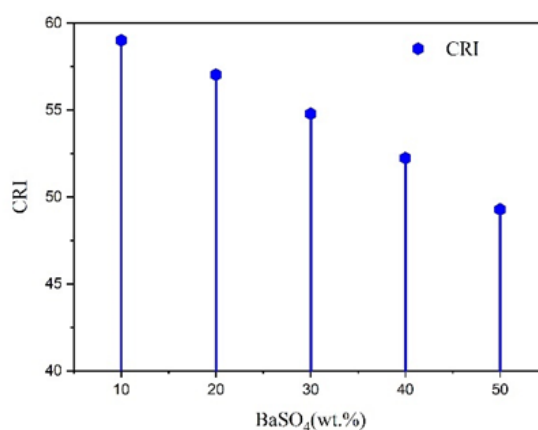
Figure 3. Influence of BaSO₄ content on the CCT valuesFigure 4. Effect of BaSO₄ proportion on the measured color deviation valuesFigure 5. Luminescence strength with various BaSO₄ proportionsFigure 6. CRI values with various BaSO₄ proportions

Table 1 compares the scattering coefficients and reduced scattering coefficients of several materials with different particle sizes. The newly investigated BaSO₄ shows a scattering coefficient of 80.35 mm⁻¹ and a reduced scattering coefficient of 11.36 mm⁻¹, values that are nearly identical to those of ZnO (80.3 and 11.4 mm⁻¹). This indicates that BaSO₄ and ZnO exhibit comparable scattering strength and

angular redistribution of light. TiO_2 , in contrast, presents a lower scattering coefficient of 40.5 mm^{-1} but the highest reduced scattering coefficient of 12.3 mm^{-1} , suggesting more effective multiple scattering. Meanwhile, CaCO_3 demonstrates much weaker scattering, with coefficients of 8.96 mm^{-1} and 0.15 mm^{-1} , placing it at the lower end of performance in this comparison.

Table 2 highlights the photometric properties of these scattering materials when incorporated into YAG: Ce^{3+} -based WLEDs. BaSO_4 achieves a YAG: Ce^{3+} ratio of 13.6% and a CCT of 6,000 K, with a relatively high D-CCT of 184.39 K. Although its CRI is moderate (46.1), its CQS (62.65) and luminous flux (174.8 lm) are high, making it a promising material for brightness enhancement. ZnO provides lower luminous flux (146.6 lm) but higher CRI (58.1), while TiO_2 shows balanced values with a CRI of 55, CQS of 61.2, and luminous flux of 142 lm. CaCO_3 , despite achieving a very high luminous flux (173.35 lm), suffers from a large D-CCT (420.59 K), which indicates poorer color stability. Together, these results suggest that BaSO_4 is a strong candidate for high-brightness WLED applications, performing on par with ZnO in scattering properties while surpassing it in luminous efficiency. However, for applications where color stability and rendering are more critical, TiO_2 or ZnO may offer a better trade-off compared with BaSO_4 and CaCO_3 .

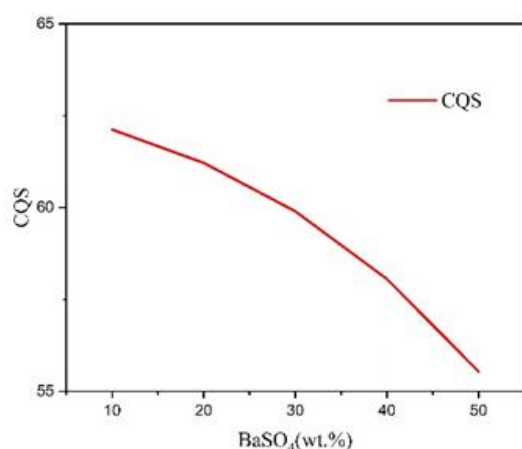


Figure 7. CQS values with various BaSO_4 proportions

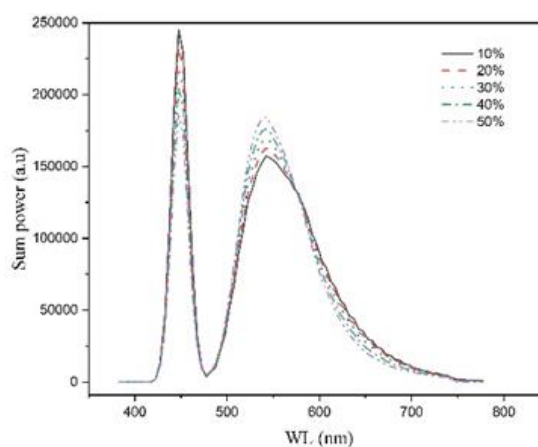


Figure 8. Luminous power of the WLED

Table 1. Result comparison of scattering coefficients influenced by particle sizes of scattering

Scattering materials	Scattering coefficients (mm^{-1})	Reduced scattering coefficients (mm^{-1})	References
BaSO_4	80.35	11.36	This work
ZnO	80.3	11.4	[19]
TiO_2	40.5	12.3	[21]
CaCO_3	8.96	0.15	[23]

Table 2. Comparative tables of this research results with reported research

Scattering materials	YAG: Ce^{3+} (%)	CCT (K)	D-CCT (K)	CRI	CQS	Lumen (lm)	References
BaSO_4	13.6	6,000	184.39	46.1	62.65	174.8	This work
ZnO	7.5	5,000	40.8	58.1	62.4	146.6	[19]
TiO_2	5.07	5,000	48.5	55	61.2	142	[21]
CaCO_3	5.95	6,000	420.59	60.17	62.6	173.35	[23]

4. CONCLUSION

In this work, PVA/ BaSO_4 nanofibers were fabricated using both conventional and ultrasonic electrospinning, with ultrasonication proving highly effective in suppressing BaSO_4 agglomeration. The particle agglomeration index slope decreased from 0.039 to 0.006, and the crystallite size was reduced from ~ 470 to ~ 300 nm, while the average fiber diameter remained unchanged. SEM, EDX, FTIR, and XRD analyses confirmed uniform nanoparticle dispersion and structural modification under ultrasonic processing. Functionally, BaSO_4 enhanced both optical and X-ray shielding performance, achieving a peak luminous flux of 174.8 lm at 50 wt%, outperforming ZnO and TiO_2 fillers. These results demonstrate the potential of

ultrasonic electrospinning for producing multifunctional PVA/BaSO₄ nanofibers suitable for radiation-protective textiles, biomedical platforms, and WLED diffusers. However, the method remains sensitive to processing variables such as frequency, viscosity, and voltage, and long-term optical stability and CRI performance were not fully investigated. Future work should therefore assess durability under continuous illumination or biomedical exposure, evaluate mechanical performance for wearable use, and explore hybrid fillers (Bi₂O₃, WO₃, and TiO₂) to balance luminous flux and CRI. Data-driven optimization of electrospinning parameters may further improve scalability and process control, enabling next-generation nanofiber systems with enhanced optical, shielding, and mechanical properties.

FUNDING INFORMATION

The authors wish to express their gratitude to the Posts and Telecommunications Institute of Technology, Vietnam, for financial support for this research.

AUTHOR CONTRIBUTIONS STATEMENT

This journal uses the Contributor Roles Taxonomy (CRediT) to recognize individual author contributions, reduce authorship disputes, and facilitate collaboration.

Name of Author	C	M	So	Va	Fo	I	R	D	O	E	Vi	Su	P	Fu
Le Thi Trang	✓	✓	✓	✓	✓	✓		✓	✓	✓			✓	✓
Nguyen Thi Phuong Loan		✓				✓		✓	✓	✓	✓	✓		
Pham Hong Cong	✓		✓	✓			✓			✓	✓		✓	✓
Nguyen Doan Quoc Anh	✓	✓	✓	✓	✓	✓		✓	✓	✓			✓	
Hsiao-Yi Lee	✓	✓	✓	✓	✓	✓		✓	✓	✓	✓		✓	✓

C : Conceptualization	I : Investigation	Vi : Visualization
M : Methodology	R : Resources	Su : Supervision
So : Software	D : Data Curation	P : Project administration
Va : Validation	O : Writing - Original Draft	Fu : Funding acquisition
Fo : Formal analysis	E : Writing - Review & Editing	

CONFLICT OF INTEREST STATEMENT

Authors state no conflict of interest.

DATA AVAILABILITY

Data availability is not applicable to this paper as no new data were created or analyzed in this study.

REFERENCES

[1] X. Dong, F. Zheng, and Z. Wang, "Research on color uniformity and seam detection of standard test paper based on machine vision," in *IMCEC 2021- EEE 4th Advanced Information Management, Communicates, Electronic and Automation Control Conference*, Jun. 2021, pp. 1391–1395, doi: 10.1109/IMCEC51613.2021.9482203.

[2] J. Chen, Z. Tian, Q. Wang, J. Liu, and Y. Mou, "Enhanced color rendering and color uniformity of PiG based WLEDs by using red phosphor lens," *IEEE Photonics Technology Letters*, vol. 33, no. 10, pp. 471–474, May 2021, doi: 10.1109/LPT.2021.3069198.

[3] Y. Qiang *et al.*, "BaO-Y2O3-Al2O3-SiO2/YAG:Ce: a novel YAG:Ce glass-ceramic with excellent fluorescent properties for phosphor-converted white LEDs," *Ceramics International*, vol. 51, no. 14, pp. 19199–19210, Jun. 2025, doi: 10.1016/j.ceramint.2025.02.097.

[4] H. Fang *et al.*, "Reactive spark plasma sintering of YAG-YAG:Ce composite phosphor ceramics for laser-driven lighting with high luminous efficacy," *Journal of Materials Chemistry C*, vol. 13, no. 9, pp. 4781–4790, 2025, doi: 10.1039/d4tc04942j.

[5] P. Greil, M. Kulig, D. Hotza, H. Lange, and R. Tischtau, "Aluminium nitride ceramics with high thermal conductivity from gas-phase synthesized powders," *Journal of the European Ceramic Society*, vol. 13, no. 3, pp. 229–237, Jan. 1994, doi: 10.1016/0955-2219(94)90031-0.




[6] O. V. Devitsky and A. A. Kravtsov, "Effect of thermal annealing on the structural evolution of thin ceramic YAG: Ce films grown by pulsed laser deposition," *Ceramics International*, vol. 51, no. 5, pp. 6011–6022, Feb. 2025, doi: 10.1016/j.ceramint.2024.12.047.

[7] B. Du, W. Li, L. Zhang, P. Chen, and F. Lu, "Recent advances in preparing transparent phosphor ceramics for high-index color rendering and high-power lighting," *Molecules*, vol. 29, no. 6, Mar. 2024, doi: 10.3390/molecules29061325.




- [8] S. Shisina, K. G. Nishanth, and S. Das, "Compositionally tuned self-activated alkali metal vanadates for high color rendering white LEDs and IR reflective pigments," *Inorganic Chemistry*, vol. 64, no. 11, pp. 5386–5404, Mar. 2025, doi: 10.1021/acs.inorgchem.4c05040.
- [9] J. Lu *et al.*, "MgO-Al₂O₃-SiO₂ glass-ceramics containing metastable MgAl₂Si₃O₁₀ phase for warm white light-emitting diodes with a high color rendering index," *Ceramics International*, vol. 51, no. 8, pp. 10877–10886, Mar. 2025, doi: 10.1016/j.ceramint.2024.12.517.
- [10] H. Chen *et al.*, "High luminous efficiency and high saturation threshold in highly transparent LuAG:Ce phosphor ceramics for laser diodes lighting," *Optics Express*, vol. 32, no. 2, Jan. 2024, doi: 10.1364/oe.510121.
- [11] G. J. Wang *et al.*, "YAG:Ce³⁺-ZnO composite phosphor-in-glass (PiG) films for high-quality laser-driven white light," *Journal of Alloys and Compounds*, vol. 1010, Jan. 2025, doi: 10.1016/j.jallcom.2024.177779.
- [12] D. Kumar, R. K. Varshney, and D. S. Mehta, "Laser-driven phosphor-converted green photonic technology based solid state lighting device for high-brightness illumination," in *Light-Emitting Devices, Materials, and Applications XXIX*, Mar. 2025, doi: 10.1117/12.3051141.
- [13] L. Huang *et al.*, "A full-spectrum color converter based on tricolor phosphor-in-glass films for laser-driven white lighting," *Journal of Materials Chemistry C*, vol. 13, no. 14, pp. 7402–7410, 2025, doi: 10.1039/d4tc05513f.
- [14] Y. Wang *et al.*, "Effect of Ga³⁺ content on the luminous properties of Ce³⁺-doped Lu₂YGa₁₅xO₁₂ phosphor ceramics for potential lighting application," *Journal of Luminescence*, vol. 280, May 2025, doi: 10.1016/j.jlumin.2025.121115.
- [15] D. Kumar, R. K. Varshney, and D. S. Mehta, "Laser-driven colour converter with Al₂O₃-ZnO composite phosphor-in-glass for high-brightness white light illumination," in *Advances in Display Technologies XV*, Mar. 2025, doi: 10.1117/12.3058138.
- [16] A. Soni and D. S. Mehta, "Diode laser-based broad spectrum solid-state lighting and visible light communication," *Optik*, vol. 327, May 2025, doi: 10.1016/j.ijleo.2025.172281.
- [17] X. Chen and X. Huang, "CaLu₂Sc₂Al₂SiO₁₂:Ce³⁺ green phosphors for high-quality white LEDs," *Inorganic Chemistry*, vol. 64, no. 5, pp. 2518–2528, Feb. 2025, doi: 10.1021/acs.inorgchem.4c05104.
- [18] Z. Yu, Y. Mou, Y. Peng, D. Chen, and M. Chen, "Toward high-brightness laser lighting: progress and perspectives on phosphor-in-glass films," *Advanced Materials Technologies*, vol. 10, no. 13, Jul. 2025, doi: 10.1002/admt.202402050.
- [19] H. T. Tung, N. D. Q. Anh, and H. Y. Lee, "Impact of phosphor granule magnitudes as well as mass proportions on the luminous hue efficiency of a coated white light-emitting diode and one green phosphor film," *Optoelectronics and Advanced Materials, Rapid Communications*, vol. 18, no. 1–2, pp. 58–65, 2024.
- [20] Q. K. Nguyen, B. Glorieux, G. Sebe, T. H. Yang, Y. W. Yu, and C. C. Sun, "Passive anti-leakage of blue light for phosphor-converted white LEDs with crystal nanocellulose materials," *Scientific Reports*, vol. 13, no. 1, Aug. 2023, doi: 10.1038/s41598-023-39929-2.
- [21] B. M. Chen, C. H. Chen, S. P. Ying, and Y. K. Chang, "Replication of leaf surface structures on flat phosphor-converted LEDs for enhanced angular color uniformity," *Micromachines*, vol. 15, no. 11, Nov. 2024, doi: 10.3390/mi15111399.
- [22] F. Wang, H. Pan, W. Mao, and D. Wang, "Optimizations of luminescent materials for white light emitting diodes toward healthy lighting," *Heliyon*, vol. 10, no. 14, Jul. 2024, doi: 10.1016/j.heliyon.2024.e34795.
- [23] H. T. Tung, D. A. N. Thi, and N. D. Q. Anh, "The effects of Ca₁₄Mg₂(SiO₄)₈:Eu²⁺ phosphor on white light emission quality of LED-phosphor packages," *Bulletin of Electrical Engineering and Informatics*, vol. 12, no. 6, pp. 3388–3394, Dec. 2023, doi: 10.11591/eei.v12i6.4792.
- [24] A. Mayavan, A. Kannan, and S. Gandhi, "Silica nanoparticles assisted Ba₂SiO₄:Eu²⁺—a bluish-green emitting remote phosphor for white light application," *Frontiers of Optoelectronics*, vol. 18, no. 1, Apr. 2025, doi: 10.1007/s12200-025-00150-w.
- [25] A. Soni, L. Pulikkool, R. Mulaveesala, S. K. Dubey, and D. S. Mehta, "Multi-color phosphor-converted wide spectrum LED light source for simultaneous illumination and visible light communication," *Photonics*, vol. 11, no. 10, Sep. 2024, doi: 10.3390/photonics11100914.

BIOGRAPHIES OF AUTHORS






Le Thi Trang    received a Master's degree in Information Technology from Lac Hong University, Vietnam, and is currently working as a lecturer at the Faculty of Information Technology, Dong Nai Technology University, Dong Nai, Vietnam. Her research interests include computer science, computer vision, image recognition and classification, face detection and recognition, abnormal motion detection, and graphic design. She can be contacted at email: lethittrang@dntu.edu.vn.






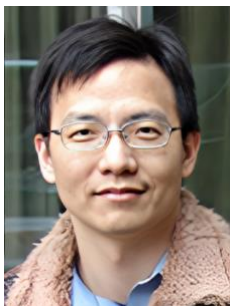
Nguyen Thi Phuong Loan    was born in Da Nang province. In 2006, she received her master's degree from the University of Natural Sciences. She received her Ph.D. degree from Ton Duc Thang University in 2024. Her research interest is optoelectronics. She has worked at the Faculty of Fundamental 2, Posts and Telecommunications Institute of Technology, Ho Chi Minh City, Vietnam. She can be contacted at email: ntploan@ptithcm.edu.vn.






Pham Hong Cong    received his M.S. in Electronic Engineering from Danang University of Science and Technology, Vietnam, in 2010. He is a lecturer at the Faculty of Electrical Engineering Technology, Industrial University of Ho Chi Minh City, Ho Chi Minh City, Vietnam. His research interests are optoelectronics (LED), power transmission, and automation equipment. He can be contacted at email: phamhongcong@iuh.edu.vn.



Nguyen Doan Quoc Anh    was born in Khanh Hoa province, Vietnam. He has been working at the Faculty of Electrical and Electronics Engineering, Ton Duc Thang University. Quoc Anh received his Ph.D. degree from National Kaohsiung University of Science and Technology, Taiwan, in 2014. His research interest is optoelectronics. He can be contacted at email: nguyendoanquocanh@tdtu.edu.vn.



Hsiao-Yi Lee    was born in Hsinchu City, Taiwan. He has been working at the Department of Electrical Engineering, National Kaohsiung University of Science and Technology, Kaohsiung, Taiwan. His research interest is optics science. He can be contacted at email: leehy@nkust.edu.tw.